Effects of Topographical and Mechanical Property Alterations Induced by Oxygen Plasma Modification on Stem Cell Behavior

Yong Yang,[†] Karina Kulangara, Ruby T. S. Lam,[‡] Rena Dharmawan,[§] and Kam W. Leong*

Department of Biomedical Engineering, Duke University, Durham, North Carolina 27708, United States. [†]Present address: Department of Chemical Engineering, West Virginia University, Morgantown, WV 26506. [‡]Present address: Nanoink, Inc., Skokie, IL 60077. [§]Present address: Duke-NUS Graduate Medical School, Singapore.

ABSTRACT Polymeric substrates intended for cell culture and tissue engineering are often surface-modified to facilitate cell attachment of most anchorage-dependent cell types. The modification alters the surface chemistry and possibly topography. However, scant attention has been paid to other surface property alterations. In studying oxygen plasma treatment of polydimethylsiloxane (PDMS), we show that oxygen plasma treatment alters the surface chemistry and, consequently, the topography and elasticity of PDMS at the nanoscale level. The elasticity factor has the predominant effect, compared with the chemical and topographical factors, on cell adhesions of human mesenchymal stem cells (hMSCs). The enhanced focal adhesions favor cell spreading and osteogenesis of hMSCs. Given the prevalent use of PDMS in biomedical device construction and cell culture experiments, this study highlights the importance of understanding how oxygen plasma treatment would impact subsequent cell–substrate interactions. It helps explain inconsistency in the literature and guides preparation of PDMS-based biomedical devices in the future.

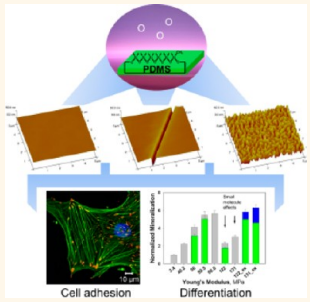

KEYWORDS: polydimethylsiloxane · oxygen plasma · nanotopography · elasticity · human mesenchymal stem cells

Polymeric substrates intended for cell culture and tissue engineering are often surface-modified to facilitate cell attachment for most anchorage-dependent cell types. The modification alters the surface chemistry[1] and probably topography.[2] However, scant attention has been paid to other surface property alterations.[3,4] In studying oxygen (O_2) plasma treatment of polydimethylsiloxane (PDMS), we show that the surface modification can alter the mechanical property of the substrate in addition to chemistry and topography, which significantly influences the behavior of human mesenchymal stem cells (hMSCs).

PDMS has seen widespread use in biological and biomedical research because of its appealing characteristics, such as biocompatibility, optical transparency, gas permeability, and rapid prototyping.[5] For instance, it is widely used to build microfluidic systems,[6–8] used as a stamp for chemical patterning to guide cell adhesion,[9–11] or fabricated with various topographical features[12–15] and elasticity[16–19] for studies of cell–substrate interactions. Because of the hydrophobic nature, the PDMS surface is usually treated with O_2 plasma to render it a hydrophilic surface to enhance protein adsorption, promote cell adhesion, or serve as nanochannels for nanofluidic manipulaton.[20,21]

In practice, not enough attention has been paid to the surface property change of PDMS after O_2 plasma treatment. Study showed that, immediately after the treatment, the contact angle dramatically dropped from 104.9 ± 3.6° of the pristine PDMS (Sylgard 184 kit, unless otherwise specified) to less than 10°, and the contact angles recovered over time by following different paths (see Figure S1 in the Supporting Information). Although enormous efforts have been made to study this process,[22–25] the understanding of this process remains incomplete and sometimes controversial due to variation in sample preparation and process parameters. Therefore, we systematically investigated the effects of O_2 plasma treatment on PDMS, in terms of chemistry, topography, and mechanical property as well as their recovery process, and examined how these changes influenced the adhesion and differentiation of hMSCs.

RESULTS AND DISCUSSION

Upon exposure to O_2 plasma, the silane ($Si-CH_3$) groups at the PDMS surface were

* Address correspondence to kam.leong@.duke.edu.

Received for review April 18, 2012 and accepted September 12, 2012.

Published online September 12, 2012
10.1021/nn301713d

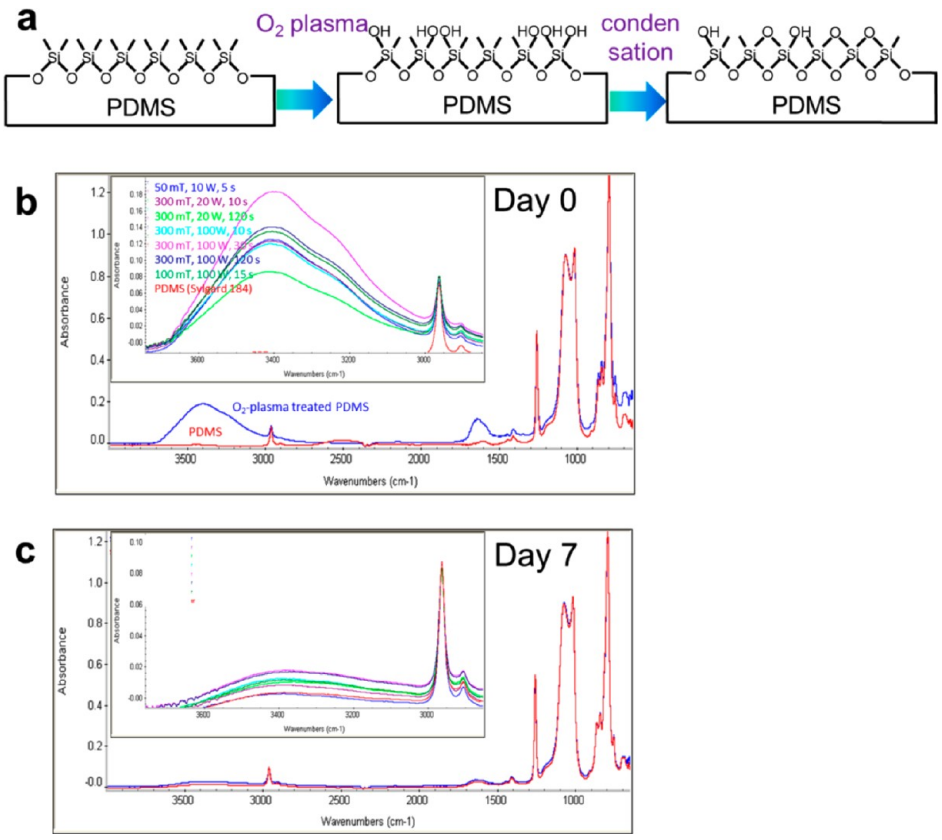

Figure 1. O_2 plasma changed the chemistry of the PDMS surface. (a) Illustrative diagram of O_2-plasma-induced oxidation of the PDMS surface. ATR-FTIR spectra of PDMS substrates (b) 10 min after the O_2 plasma treatment and (c) aged at ambient conditions for 7 days.

converted to silanol (Si-OH) groups and the surface became hydrophilic (Figure 1a). The resultant silanol groups might condense with the neighboring silanol groups to form a brittle layer where silicon might be bonded to three or four oxygen atoms (SiO_x).[24] Attenuated total reflection-Fourier transform infrared (ATR-FTIR) spectra showed that, compared with pristine PDMS, the plasma-treated PDMS surface exhibited clear hydroxyl bands. The key plasma process parameters are radio frequency (RF) power (watt or W), chamber pressure (millitorr or mT; 1 mT = 0.133 Pa), and exposure time (s). The RF power and chamber pressure determine the plasma intensity. The exposure time defines the plasma dosage. Depending on the process parameters, the bands had different amplitudes (Figure 1b). After 7 days, the difference in the hydroxyl band between these PDMS surfaces was undetectable (Figure 1c).

We further examined the topography of the PDMS surfaces using atomic force microscopy (AFM) (Figure 2). The pristine PDMS had a smooth surface with a root mean square (rms) roughness of 0.65 nm. After exposure to plasma at low intensity (300 mT, 20 W) for 10−30 s, the surface became even smoother (rms = 0.24 nm), attributed to the conversion of the silicon structure to SiO_x-rich structure, thereby reducing the specific volume and smoothing the surface layer. However, with a prolonged exposure time (120 s), straight cracks were observed because the prolonged densification of the SiO_x layer led to a buildup of tensile stress.[24] Note that similar topography could be rendered using different combinations of process parameters. For instance, a smooth surface was generated at 50 mT and 10 W for 5 s, and a cracked surface at 300 mT and 50 W for 30 s. The advance in scanning probe microscopy enables us to map topography and elasticity simultaneously in a single scan.[26,27] On the cracked surface, the elasticity mapping revealed that the smooth surface outside the crack had a Young's modulus (elasticity) of 46.4 $\pm$ 4.2 MPa, 12 times higher than that of pristine PDMS, 3.4 $\pm$ 0.2 MPa (Figure 2a), confirming the formation of a stiffer layer. At the bottom of the crack, the elasticity was 9.2 MPa, between the values of the stiffer layer and the pristine PDMS. Continuous exposure of the PDMS surface to plasma resumed the oxidation but did not change the quantity of the cracks as observed up to 30 min (data not shown).

At high plasma intensity (300 mT and 100 W), wiggled cracks formed even at an exposure time as short as 10 s. More cracks formed, and the surface became rough over time. The roughness increased as a function of the exposure time. Again, a similar rough surface was formed with a different parameter set

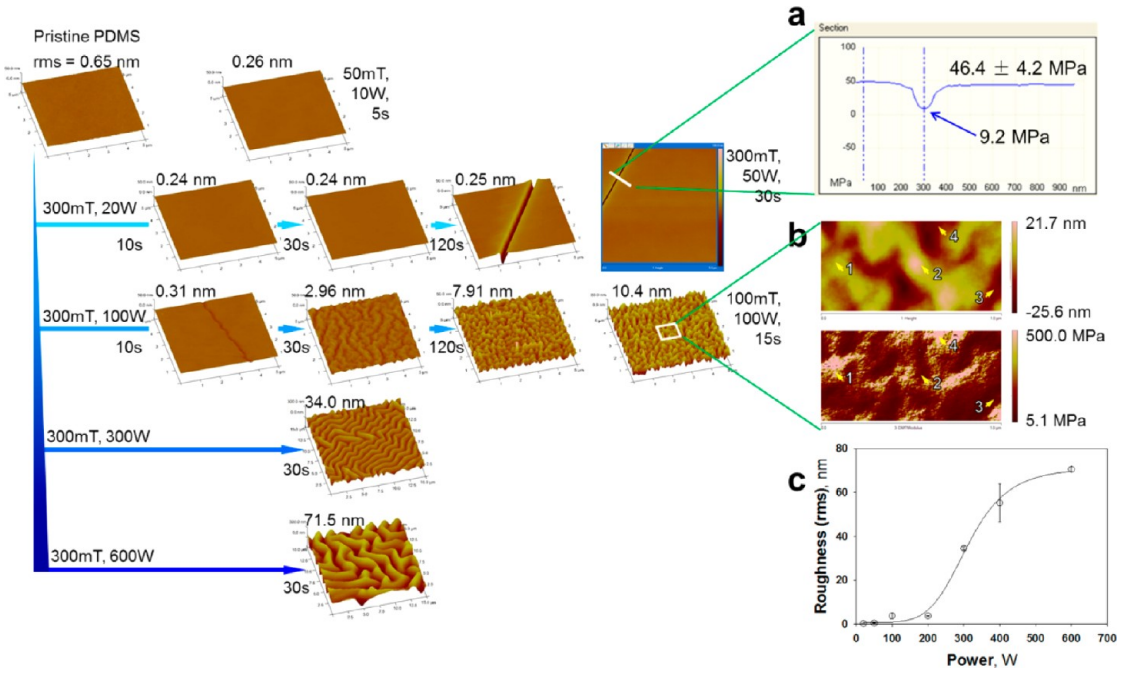

Figure 2. O_2 plasma oxidation altered the topography of PDMS surfaces. The effects of the plasma treatment on the topography of PDMS substrates were summarized: the evolution of topography as a function of exposure time was demonstrated along the horizontal direction, while the influence of plasma intensity on topography was exhibited vertically. The scanning scale for all of the images was 5 μm except two cases: 300 mT, 300 W for 30 s and 300 mT, 600 W for 30 s, which had a scanning size of 15 μm. (a) Young's modulus curve across a crack. The inspection line was indicated by the white line over the 2-D image of the PDMS surface plasma-treated at 300 mT and 50 W for 30 s. (b) Topography (top panel) and Young's modulus (bottom panel) images over a 1 μm $\times$ 1 μm area of the PDMS surface plasma-treated at 100 mT and 100 W for 15 s. (c) Surface roughness as a function of the RF power. The chamber pressure and the exposure time were kept unchanged: 300 mT and 30 s, respectively. The roughness increased when the RF power increased. The curve through the data points is for visual guide only.

(100 mT, 100 W, 15 s). A close examination at 1 μm scale showed that there was no correspondence between the topography and elasticity (Figure 2b). For example, the topographical peaks (spots 1 and 2) could be either a peak (spot 1) or a valley (spot 2) in elasticity, or the topographical valley (spots 3 and 4) could be a valley (spot 3) or peak (spot 4) in elasticity. It was postulated that the high plasma intensity resulted in sudden chemical change and drastic buildup of the stress locally, which generated enormous cracks, similar to the formation of the cracks on dried mud. Due to the smaller size, usually at the nanoscale, the cracked surface might go through reconstruction and form a mixture of soft silicon pieces and rigid SiO_x-rich pieces. Therefore, the elasticity (Young's modulus) is independent of topography.

When the exposure time was fixed at 30 s, the surface roughness, compared with the pristine PDMS, changed from smoother surfaces to rougher surfaces, depending on the energy input (Figure 2c). In addition, through regulation of the relief of the plasma-induced residual stress using micropatterns, regular nano- and microscale patterns could be formed (Figure S2).[28] In brief, by changing the plasma parameters, smooth, cracked, or rough surfaces could be generated as evidenced in the SEM observations (Figure S3).

Being thermodynamically unstable, the topography recovered over time (Figure 3). On a smooth surface (Figure 3a), the sparsely distributed nanoscale drops appeared on the surface slowly, resulting in a slight increase in the roughness. The dark spots in the phase image indicated soft materials. Previous studies indicate that these soft materials are low molecular weight (LMW) molecules including un-cross-linked PDMS molecules and the residual curing agent.[24,25,29] Because the LMW molecules had to diffuse through the dense SiO_x layer from the interior to the surface, the recovery was slow. The scenario was different when cracks formed. Figure 3b shows that LMW molecules appeared preferentially surrounding the cracks, coalesced, spread, and covered more surface area over time. The cracks provided a locus for the surface-tension-driven diffusion of LMW molecules.[23] The rough surface also provided the enormous openings for the diffusion, and the roughness decreased in an exponential manner (Figure 3c). It was noticed that the migration of LMW molecules was expedited by the frequent scanning of the AFM tip (Figure S4). Nevertheless, it was clear that topographical recovery was affected by the diffusion of LMW molecules, ultimately dependent on the plasma process parameters.

Equally important, plasma oxidation altered the elasticity of the PDMS surface (Figure 4). Because oxidation converted the soft silicon structure to the stiff SiO_x structure, the more the surface was oxidized,

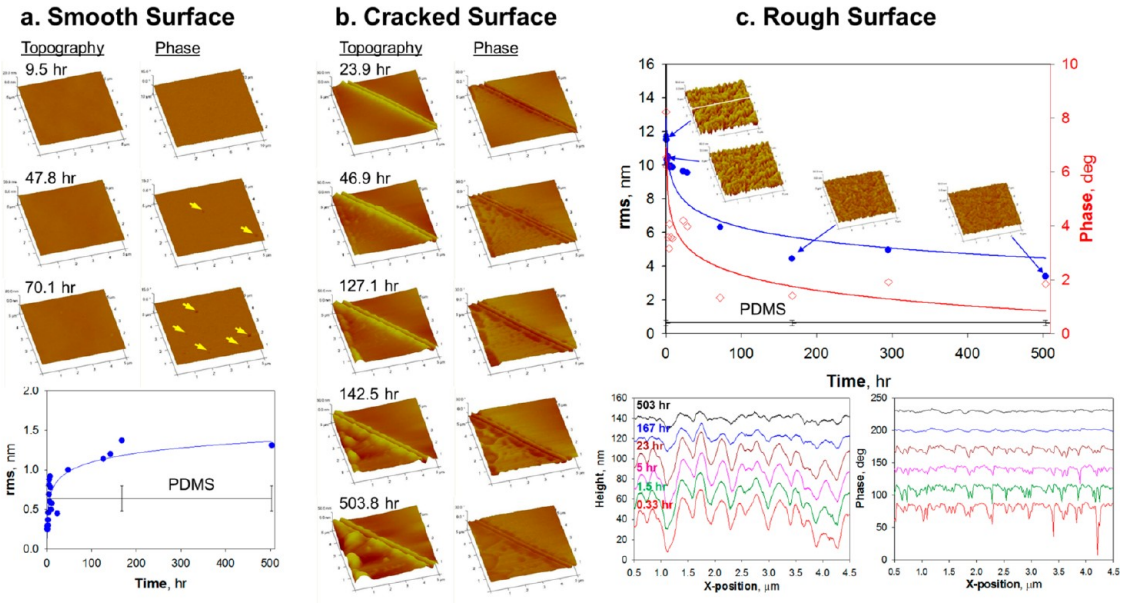

Figure 3. Topographical recovery of the oxidized PDMS surfaces. The PDMS substrates in both (a) and (b) were oxidized at 300 mT and 20 W for 120 s. (a) Recovery of a smooth surface away from the crack; 9.5 h after the treatment, no detectable changes were observed on both topography and phase images. After 47.8 h, two light dark spots (yellow arrows) were observed in the phase image. At 70.1 h, these two spots became darker and more spots were observed. The change of the roughness over a scanning scale of 5 μm was summarized in the plot. (b) Recovery of a cracked surface. The images in the left and right columns were topography and phase images, respectively. At 23.9 h after treatment, dark spots appeared along the crack in the phase image, indicating that LMW molecules diffused from the interior to the surface. At 46.9 h, more LMW molecules diffused out and spread. Over time, the dark spots coalesced and covered a larger area. (c) Recovery of a rough surface oxidized at 100 mT and 100 W for 15 s. The top panel summarizes the recovery at a scanning size of 5 μm over 3 weeks, exemplified by some representative 3-D topography images. The black horizontal line indicates the roughness of the pristine PDMS. The lower panels were the topographical (lower left) and phase (lower right) profiles which were taken from a representative line, as labeled with the white line in the 3-D topography in the top panel. These profiles were aligned horizontally and offset vertically for clarity. Right after the treatment, the surface was rough, as indicated with the peaks and valleys. The magnitude of the fluctuation decreased over time.

the stiffer the surface became. The stiffer layer may be up to several hundred nanometers in thickness.[30] Smooth surfaces had narrower modulus distribution than that of rough surfaces. Over time, the elasticity of PDMS surfaces decreased because the LMW molecules diffused out and accumulated at the surface. In summary, O_2 plasma oxidation altered the surface chemistry and, consequently, the topography and elasticity of PDMS at the nanoscale level.

We next investigated the response of hMSCs to the nanoscale property alterations. The cells were seeded on the PDMS surfaces without protein coating (Figure 5a). After 7 days of culture, hMSCs exhibited a higher density on the treated PDMS surfaces than that on the pristine PDMS (see Table S1 in Supporting Information); the cells formed distinct cell adhesion complexes (paxillin-labeled) and developed mature stress fibers on the treated surfaces, while the cell adhesions were diffuse on the pristine PDMS. The difference in cell adhesions was quantitatively assessed using Western blot. There was no correspondence between paxillin expression and the roughness. Strikingly, the amount of paxillin monotonically increased as a function of the Young's modulus; there was about 4-fold increase when the Young's modulus increased from 3.4 to 131 MPa (Figure 5b). The difference in paxillin could not be attributed to the surface chemistry because the chemistry of these substrates at day 7 was similar to that of pristine PDMS (Figure 1c). Evidently, the substrate elasticity, instead of topography or surface chemistry, was the major regulator of cell adhesion complexes. This elasticity effect was alleviated when the PDMS substrates were precoated with type I collagen (Figure S5).

Further, this elasticity effect on different stages of cell adhesion was investigated by immunostaining the nascent focal complexes Arp2/3[31] and mature focal adhesions zyxin.[32] Arp2/3 was stained primarily around the periphery of the cells, and no obvious difference was detected (Figure S6). Zyxin was diffuse on the pristine PDMS but became distinct with increasing elasticity (Figure S7). Western blot analysis (Figure 5c) showed that the Arp2/3 expression was independent of the elasticity; however, zyxin increased with an increase in Young's modulus up to 50 MPa and leveled off afterward.

Notably, there was a drop of zyxin for the freshly prepared cracked and rough PDMS surfaces, 122 and 131 MPa; in contrast, on the same substrates but aged for 7 days (*i.e.*, 96.6 and 59.5 MPa), the zyxin expression was higher. Considering that the freshly prepared DPMS surfaces went through a quick recovery initially

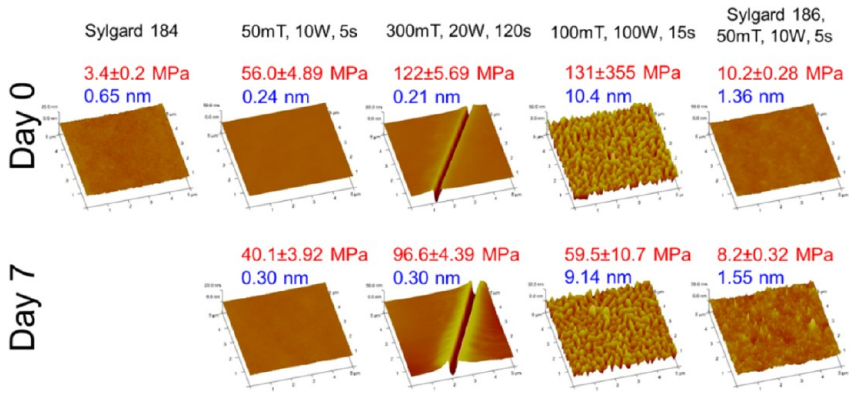

Figure 4. Plasma oxidation induced the elasticity change of the PDMS surfaces. The PDMS surfaces were plasma-treated at different conditions, and the AFM measurements were conducted right after the plasma treatment as Day 0 or aged for 7 days as Day 7. The 3-D topographies of the oxidized PDMS surfaces tagged with the Young's modulus and roughness are presented. All of the substrates were Sylgard 184, except the substrates in the last column, which were Sylgard 186. The Young's modulus of pristine Sylgard 186 is 0.7 MPa.

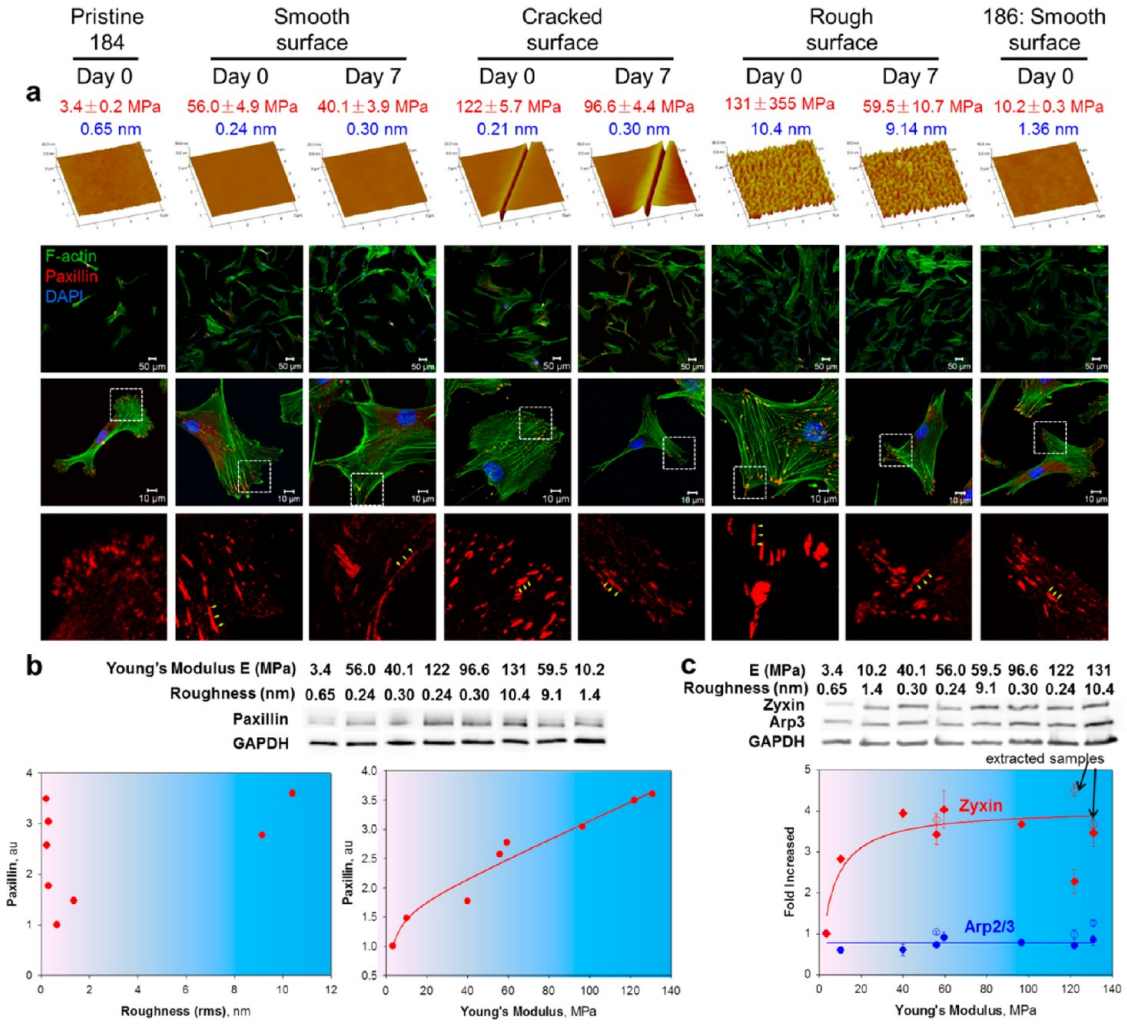

Figure 5. Surface property alterations induced by plasma oxidation influenced cell adhesions of hMSCs. (a) hMSCs adhered to the PDMS surfaces with a broad spectrum of elasticity and roughness. The first row AFM images showed the 3-D topography of the PDMS substrates, tagged with the Young's modulus and roughness. The second row showed that hMSCs had different density and spreading on the PDMS substrates. The third row exhibited cell morphology and cytoskeleton organization of hMSCs, and the paxillin-labeled focal adhesions in the boxed regions are enlarged in row 4. The yellow arrowheads point to the cell adhesion. (b) Western blot analysis of paxillin, which was plotted as the function of roughness and Young's modulus. (c) Western blot analysis of Arp2/3 and zyxin in hMSCs on the PDMS substrates. The hexane-extracted PDMS substrates are labeled using open diamonds. For the Western blot analysis, the band intensity was normalized based on GAPDH and compared with that in the hMSCs on the pristine PDMS surface.

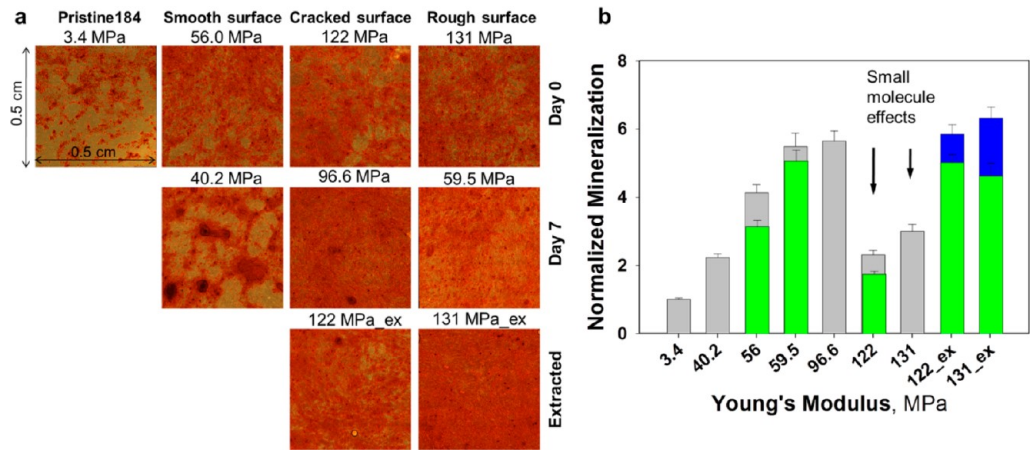

Figure 6. Osteogenesis of hMSCs on the PDMS substrates. (a) Alizarin red staining of hMSCs on the PDMS surfaces. The labels with suffix "_ex" were substrates extracted with hexane for 72 h before O_2 plasma treatment. The scanning area is 0.5 cm × 0.5 cm. (b) Quantification of cell mineralization. The gray bars represent the PDMS substrates, the blue ones the extracted substrates, and the green ones denote when Y-27632 was added. Error bars represent means ± SD for $n = 3$.

(Figure 3b,c) while the aged ones were more stable, we postulated that the LMW molecules diffusing to the surface act as a "lubricant" to hamper the formation of focal adhesions (Figure S8). The PDMS substrates were thus Soxhlet extracted with hexane for 72 h before the plasma treatment. The hMSCs grown on the extracted substrates exhibited a higher zyxin expression, matching the general trend, as indicated with open diamond symbols in Figure 5c.

This plasma-altered substrate elasticity and the lubricated surface have a pronounced effect on cell phenotypes such as osteogenesis of hMSCs (Figure 6). Cell mineralization was evaluated by alizarin red S staining (Figure 6a) and further quantitatively assessed (Figure 6b). Osteogenesis was enhanced with an increase in Young's modulus and also depressed for 122 and 131 MPa because LMW molecules hampered the formation of mature focal adhesions. Extraction of the LMW molecules brought the osteogenesis to the normal trend. In this study, the cells reached confluence after 3 weeks, and the substrate elasticity mediated the intracellular contractility through the mechanosensory component such as zyxin, thus affecting cell differentiation. Y-27632, an inhibitor of Rho kinase, was then added to evaluate the influence of intracellular contractility on osteogenesis. As expected, the addition of Y-27632 lowered the level of osteogenesis (Figure 6), confirming the effect of O_2 plasma treatment and ultimately intracellular contractility on osteogenesis of hMSCs.

CONCLUSIONS

In this study, we showed that the O_2 plasma treatment altered the surface chemistry and, consequently, the nanoscale topography and elasticity of PDMS. The elasticity factor had the predominant effect, compared with the chemical and topographical factors, on cell adhesions of hMSCs. The enhanced focal adhesions favored cell spreading and osteogenesis of hMSCs. The diffusion of LMW molecules diffusing from the interior to the surface also influenced the surface topography and elasticity, which had an inverse impact on focal adhesions and osteogenesis. Given the prevalent use of PDMS in biomedical device construction and cell culture experiments, this study highlights the importance of understanding how O_2 plasma treatment would impact subsequent cell−substrate interactions. It helps explain inconsistency in the literature and guides preparation of PDMS-based biomedical devices in the future.

MATERIALS AND METHODS

PDMS and O_2 Plasma Treatment. PDMS resin and curing agent (Sylgard 184 kit, Dow Corning; unless otherwise specified) with a weight ratio of 10:1.05 were thoroughly mixed, degassed, and poured onto a 150 mm polystyrene Petri dish (Becton, Dickinson and Company). Different from the manufacturer recommended ratio of 10:1, a slightly higher concentration of curing agent was added to reduce the amount of uncured oligomers.[33] After curing for 2 h at 75 °C, the ~2 mm thick PDMS plate was punched into discs of two diameters, 1.5 and 2.2 cm, for 24-well and 12-well plates, respectively.

Some discs were extracted with hexanes using the Soxhlet extractor for 72 h. Upon completion of the extraction, the discs were sandwiched between two clean glass plates overnight in a chemical hood until the discs deswelled. These discs were then placed in a vacuum oven at 70 °C before the plasma treatment.

The discs, with the free surface facing up, were exposed to oxygen plasma under predetermined conditions in a Phantom II reactive ion etch (RIE)/inductively coupled plasma (ICP) generator (600 W, 13.56 MHz) from Trion Technology, Inc., USA. The discs were placed at the center of the chamber to achieve a uniform plasma exposure. The freshly treated samples were labeled at day 0. At the end of the first day of aging, the samples were labeled as day 1. Following this way, the samples aged at the end of 7 days were labeled at day 7.

Contact Angle Measurement. The contact angles of deionized water on PDMS substrates were measured in the static mode using a Rame-Hart model 100 contact angle goniometer (Ramé-Hart Instrument Co., NJ, USA). Coverslip was used to support the PDMS substrates to eliminate the possible disturbance from bending the substrates. Droplets of about 3 μL (the diameter of a spherical droplet is about 1.8 mm) were gently deposited on the substrate using a micropipet. Three to six measurements were taken at different locations on the substrate, and the average was reported.

Attenuated Total Reflection-Fourier Transform Infrared Spectroscopy (ATR-FTIR). ATR-FTIR spectra were recorded on a Nicolet iS10 FTIR spectrometer with a Smart Multi-Bounce Flat HATR. The PDMS samples were clamped on a germanium reflection element, and 64 infrared spectra were averaged in the 600−4000 cm^{-1} spectra range, with 4 cm^{-1} resolution. The angle of the Ge element is 45°, and its refractive index is 4.0. Taking the refractive index of 1.4 for PDMS, the depth of penetration is about 2 μm for the wavenumber of 3000 cm^{-1} and 0.66 μm for 1000 cm^{-1}.

Atomic Force Microscopy. AFM characterization was performed using a Digital Instruments Dimension 3100 scanning probe microscope in the tapping mode under ambient conditions. Topography and phase images were recorded simultaneously at the fundamental resonance frequency of the cantilever, with a typical scan rate of 1 Hz and a resolution of 512 samples per line. The roughness reported has been measured for a $5 \times 5\ \mu m^2$ area and corresponds to the root mean square (rms) value of the surface heights. The mechanical property mapping was conducted in HarmoniX mode in Veeco Metrology Inc. (Santa Barbara, CA, USA).

Cell Culture. The hMSCs were supplied by Dr. D. Prockop from Tulane Center for Gene Therapy at Tulane University, New Orleans, LA. The hMSCs used in the experiments were at passage 3−6. The hMSCs were cultured in complete culture media (CCM) comprising α-minimum essential medium (α-MEM) supplemented with 16.5% (v/v) fetal bovine serum (FBS, Atlanta Biologicals, Inc., Lawrenceville, GA, USA), 2 mM L-glutamine (Gibco/Invitrogen, Carlsbad, CA, USA), 100 U/mL penicillin, and 100 mg/mL streptomycin (Gibco/Invitrogen, Carlsbad, CA, USA).

For osteogenic differentiation, hMSCs were cultured in CCM for a week before being changed to osteogenic differentiation media (CCM supplemented with 10 nM dexamethasone, 20 mM β-glycerolphosphate, and 50 μM L-ascorbic acid 2-phosphate). Three weeks later, the cells were fixed for alizarin staining. The chemicals used are from Sigma-Aldrich Co., St. Louis, MO, USA.

The cell seeding densities were 12 000 cells/cm^2 for focal adhesion assays (immunofluorescence staining and Western blot) and 20 000 cells/cm^2 for differentiation assay.

Immunofluorescence Staining. Human MSCs were fixed in 4% parafomaldehyde in phosphate buffered saline (PBS, Mediatech, Inc., Herndon, VA) for 15 min at room temperature and rinsed with PBS three times. The cells were permeabilized in a blocking solution, which consists of 0.03 g/mL bovine serum albumin (BSA, Sigma-Aldrich Co.) and 0.1% goat serum (Sigma-Aldrich Co.) in 0.2% Triton X-100 (Sigma-Aldrich Co.) in PBS for 1 h. Samples were then incubated with primary antibodies at room temperature for 2 h. The concentrations of the antibodies were 1:200 for antipaxillin (Epitomics, Inc., Burlingame, CA, USA), 1:100 for anti-Arp3 (Abcam Inc., Cambridge, MA, USA) and 1:100 for antizyxin (Abcam Inc.). Upon completion, the samples were washed with fresh PBS five times, 10 min each, to remove nonspecific charges and minimize background labeling. A secondary, biotin-conjugated antibody (Alexa-Fluor488 goat anti-mouse antibody at 1:200 or Alexa-Fluor 546 goat anti-rabbit antibody from Molecular Probes, Invitrogen Co., Carlsbad, CA, USA) was added for 1 h at room temperature, followed by subsequent washing as described above. F-actin was fluorescent-stained with Oregon Green 488 phalloidin (Molecular Probes). The nuclei of the cells were stained with 4,6-diamidino-2-phenylindole (DAPI, Molecular Probes) for 15 min, at room temperature, followed by final washing steps described above. The samples were then mounted in Fluoro-Gel (Electron Microscopy Sciences, Hatfield, PA, USA) for fluorescent imaging and viewed with Zeiss LSM 510 inverted confocal microscope.

Cell Density Analysis. Human MSCs were cultured on PDMS substrates for 7 days, fixed, and stained with DAPI as described above. Fluorescence images were taken using 10× or 20× objectives and analyzed using ImageJ (open source image analysis software, downloaded from http://rsb.info.nih.gov/ij/index.html). The nuclei were highlighted by adjusting threshold of the brightness, outlined, and counted by using "Analyze Particles" function. The cell density was expressed as mean ± standard error from 4 to 8 measurements.

Western Blot. After 7 days culture in CCM, the cells were harvested and lysed in cold RIPA lysis buffer (Santa Cruz Biotechnology, Inc., CA, USA). Proteins were separated by using Ready Gel Tris-HCl gel (Bio-Rad Laboratories, Inc., Hercules, CA, USA) and transferred to nitrocellulose membranes (BioRad), blocked with 5% in TBST 0.1% (1× TBS + 0.1% Tween 20), immunoblotted with specific primary antibodies: mouse antizyxin diluted at 1:1000, mouse anti-Arp3 antibody diluted 1:1000, rabbit antipaxillin diluted at 1:1000, and mouse anti-GAPDH diluted 1:800 (Abcam Inc.), and detected using horseradish peroxidase-conjugated secondary antibodies (BioRad) and Amersham ECL Plus (GE Healthcare, Piscataway, NJ, USA) as a chemiluminescent substrate. GAPDH was used as a loading control.

Densitometric analysis was performed using an Alpha-Innotech imaging system (Fluorchem FC2). The protein bands were corrected against GAPDH, compared with those in cells cultured on pristine PDMS, and plotted with respect to the roughness or Young's modulus.

Osteogenesis: Alizarin Red S (ARS) staining. To evaluate mineralized matrix (osteogenesis), hMSCs were fixed with 4% formaldehyde for 1 h and stained with 1% alizarin-red S (Sigma-Aldrich) solution in water for 20 min. After staining, the samples were washed several times to minimize nonspecific, background staining and viewed under Nikon Eclipse TE 2000-U inverted microscope. Each image taken was a collection of 14 × 19 smaller images taken with the 20× objective, thus the resultant large image measures about 0.5 cm by 0.5 cm.

ARS staining was further quantitatively assessed according to a published protocol.[34] Briefly, 400 μL of 10% (v/v) acetic acid was added onto each well of 12-well plates for 30 min with shaking. The monolayer was scraped from the PDMS discs and transferred into a 1.5 mL microcentrifuge tube. The tube was heated to 85 °C for 10 min and then centrifuged at 20 000*g* for 15 min. Then, 250 μL of the supernatant was transferred into a new 1.5 mL tube and neutralized by the additional 100 μL of ammonium hydroxide (10% v/v). Aliquots (150 μL) of the supernatant were read in triplicate at 405 nm in 96-well format with a spectrophotometric microplate reader (Bio-Rad 680, USA). The readouts were normalized based on that of pristine PDMS.

To evaluate the influence of intracellular contractility on osteogenesis, Y-27632 was then added at 2 μM every another day. After 3 weeks, no obvious difference was observed in cell spread and morphology when compared with those without the inhibitor.

Conflict of Interest: The authors declare no competing financial interest.

Acknowledgment. The authors would like to acknowledge S. Hu at Veeco Metrology Inc. for help with the Harmonix measurements, B. Anderson at Thermo North America LLC for help with ATR-FTIR measurements, B. O'Grady in Trion Technology for helpful discussion on oxygen plasma treatment, and the funding support from the National Institutes of Health (HL83008, EB15300).

Supporting Information Available: Supplemental figures. This material is available free of charge *via* the Internet at http://pubs.acs.org.

REFERENCES AND NOTES

1. Niklason, L. E.; Gao, J.; Abbott, W. M.; Hirschi, K. K.; Houser, S.; Marini, R.; Langer, R. Functional Arteries Grown *in Vitro*. *Science* **1999**, *284*, 489–493.

2. Miller, D. C.; Thapa, A.; Haberstroh, K. M.; Webster, T. J. Endothelial and Vascular Smooth Muscle Cell Function on Poly(lactic-*co*-glycolic acid) with Nano-structured Surface Features. *Biomaterials* **2004**, *25*, 53–61.
3. Torres, J. M.; Stafford, C. M.; Vogt, B. D. Manipulation of the Elastic Modulus of Polymers at the Nanoscale: Influence of UV-Ozone Cross-Linking and Plasticizer. *ACS Nano* **2010**, *4*, 5357–5365.
4. Thompson, M. T.; Berg, M. C.; Tobias, I. S.; Lichter, J. A.; Rubner, M. F.; Van Vliet, K. J. Biochemical Functionalization of Polymeric Cell Substrata Can Alter Mechanical Compliance. *Biomacromolecules* **2006**, *7*, 1990–1995.
5. Duffy, D. C.; McDonald, J. C.; Schueller, O. J. A.; Whitesides, G. M. Rapid Prototyping of Microfluidic Systems in Poly(dimethylsiloxane). *Anal. Chem.* **1998**, *70*, 4974–4984.
6. Kenis, P. J. A.; Ismagilov, R. F.; Whitesides, G. M. Microfabrication Inside Capillaries Using Multiphase Laminar Flow Patterning. *Science* **1999**, *285*, 83–85.
7. Ionescu-Zanetti, C.; Shaw, R. M.; Seo, J.; Jan, Y.-N.; Jan, L. Y.; Lee, L. P. Mammalian Electrophysiology on a Microfluidic Platform. *Proc. Natl. Acad. Sci. U.S.A.* **2005**, *102*, 9112–9117.
8. Gu, W.; Zhu, X.; Futai, N.; Cho, B. S.; Takayama, S. Computerized Microfluidic Cell Culture Using Elastomeric Channels and Braille Displays. *Proc. Natl. Acad. Sci. U.S.A.* **2004**, *101*, 15861–15866.
9. Thery, M.; Jimenez-Dalmaroni, A.; Racine, V.; Bornens, M.; Julicher, F. Experimental and Theoretical Study of Mitotic Spindle Orientation. *Nature* **2007**, *447*, 493–496.
10. McBeath, R.; Pirone, D. M.; Nelson, C. M.; Bhadriraju, K.; Chen, C. S. Shape Cell Cytoskeletal Tension, and RhoA Regulate Stem Cell Lineage Commitment. *Dev. Cell* **2004**, *6*, 483–495.
11. Kilian, K. A.; Bugarija, B.; Lahn, B. T.; Mrksich, M. Geometric Cues for Directing the Differentiation of Mesenchymal Stem Cells. *Proc. Natl. Acad. Sci. U.S.A.* **2010**, *107*, 4872–7.
12. Kurpinski, K.; Chu, J.; Hashi, C.; Li, S. Anisotropic Mechanosensing by Mesenchymal Stem Cells. *Proc. Natl. Acad. Sci. U.S.A.* **2006**, *103*, 16095–16100.
13. Bettinger, C. J.; Zhang, Z.; Gerecht, S.; Borenstein, J. T.; Langer, R. Enhancement of *In Vitro* Capillary Tube Formation by Substrate Nanotopography. *Adv. Mater.* **2008**, *20*, 99–103.
14. Bian, W.; Liau, B.; Badie, N.; Bursac, N. Mesoscopic Hydrogel Molding To Control the 3D Geometry of Bioartificial Muscle Tissues. *Nat. Protoc.* **2009**, *4*, 1522–1534.
15. Gerecht, S.; Bettinger, C. J.; Zhang, Z.; Borenstein, J. T.; Vunjak-Novakovic, G.; Langer, R. The Effect of Actin Disrupting Agents on Contact Guidance of Human Embryonic Stem Cells. *Biomaterials* **2007**, *28*, 4068–4077.
16. Fuard, D.; Tzvetkova-Chevolleau, T.; Decossas, S.; Tracqui, P.; Schiavone, P. Optimization of Poly-di-methyl-siloxane (PDMS) Substrates for Studying Cellular Adhesion and Motility. *Microelectron. Eng.* **2008**, *85*, 1289–1293.
17. Saez, A.; Ghibaudo, M.; Buguin, A.; Silberzan, P.; Ladoux, B. Rigidity-Driven Growth and Migration of Epithelial Cells on Microstructured Anisotropic Substrates. *Proc. Natl. Acad. Sci. U.S.A.* **2007**, *104*, 8281–8286.
18. du Roure, O.; Saez, A.; Buguin, A.; Austin, R. H.; Chavrier, P.; Siberzan, P.; Ladoux, B. Force Mapping in Epithelial Cell Migration. *Proc. Natl. Acad. Sci. U.S.A.* **2005**, *102*, 2390–2395.
19. Fu, J.; Wang, Y. K.; Yang, M. T.; Desai, R. A.; Yu, X.; Liu, Z.; Chen, C. S. Mechanical Regulation of Cell Function with Geometrically Modulated Elastomeric Substrates. *Nat. Methods* **2010**, *7*, 733–6.
20. Zhu, X.; Mills, K. L.; Peters, P. R.; Bahng, J. H.; Liu, E. H.; Shim, J.; Naruse, K.; Csete, M. E.; Thouless, M. D.; Takayama, S. Fabrication of Reconfigurable Protein Matrices by Cracking. *Nat. Mater.* **2005**, *4*, 403–406.
21. Huh, D.; Mills, K. L.; Zhu, X.; Burns, M. A.; Thouless, M. D.; Takayama, S. Tuneable Elastomeric Nanochannels for Nanofluidic Manipulation. *Nat. Mater.* **2007**, *6*, 424–428.
22. Owen, M. J.; Smith, P. J. Plasma Treatment of Polydimethylsiloxane. *J. Adhes. Sci. Technol.* **1994**, *8*, 1063–1075.
23. Fritz, J. L.; Owen, M. J. Hydrophobic Recovery of Plasma-Treated Polydimethylsiloxane. *J. Adhes.* **1995**, *54*, 33–45.
24. Hillborg, H.; Ankner, J. F.; Gedde, U. W.; Smith, G. D.; Yasuda, H. K.; Wikstrom, K. Crosslinked Polydimethylsiloxane Exposed to Oxygen Plasma Studied by Neutron Reflectometry and Other Surface Specific Techniques. *Polymer* **2000**, *41*, 6851–6863.
25. Eddington, D. T.; Puccinelli, J. P.; Beebe, D. J. Thermal Aging and Reduced Hydrophobic Recovery of Polydimethylsiloxane. *Sens. Actuators, B* **2006**, *B114*, 170–172.
26. Sahin, O. Scanning below the Cell Surface. *Nat. Nanotechnol.* **2008**, *3*, 461–462.
27. Sahin, O.; Erina, N. High-Resolution and Large Dynamic Range Nanomechanical Mapping in Tapping-Mode Atomic Force Microscopy. *Nanotechnology* **2008**, *19*, 445717/1–445717/9.
28. Bowden, N.; Huck, W. T. S.; Paul, K. E.; Whitesides, G. M. The Controlled Formation of Ordered, Sinusoidal Structures by Plasma Oxidation of an Elastomeric Polymer. *Appl. Phys. Lett.* **1999**, *75*, 2557–2559.
29. Hillborg, H.; Tomczak, N.; Olah, A.; Schoenherr, H.; Vancso, G. J. Nanoscale Hydrophobic Recovery: A Chemical Force Microscopy Study of UV/Ozone-Treated Cross-Linked Poly(dimethylsiloxane). *Langmuir* **2004**, *20*, 785–794.
30. Mills, K. L.; Zhu, X.; Takayama, S.; Thouless, M. D. The Mechanical Properties of a Surface-Modified Layer on Polydimethylsiloxane. *J. Mater. Res.* **2008**, *23*, 37–48.
31. Ridley, A. J.; Schwartz, M. A.; Burridge, K.; Firtel, R. A.; Ginsberg, M. H.; Borisy, G.; Parsons, J. T.; Horwitz, A. R. Cell Migration: Integrating Signals from Front to Back. *Science* **2003**, *302*, 1704–1709.
32. Geiger, B.; Spatz, J. P.; Bershadsky, A. D. Environmental Sensing through Focal Adhesions. *Nat. Rev. Mol. Cell Biol.* **2009**, *10*, 21–33.
33. Lee, J. N.; Park, C.; Whitesides, G. M. Solvent Compatibility of Poly(dimethylsiloxane)-Based Microfluidic Devices. *Anal. Chem.* **2003**, *75*, 6544–6554.
34. Gregory, C. A.; Gunn, W. G.; Peister, A.; Prockop, D. J. An Alizarin Red-Based Assay of Mineralization by Adherent Cells in Culture: Comparison with Cetylpyridinium Chloride Extraction. *Anal. Biochem.* **2004**, *329*, 77–84.